Bony ingrowth potential of 3D-printed porous titanium alloy: a direct comparison of interbody cage materials in an in vivo ovine lumbar fusion model

Kirk C. McGilvray, PhD[a,*], **Jeremiah Easley, DVM**[b], **Howard B. Seim, DVM**[b], **Daniel Regan, DVM,PhD**[a], **Sigurd H. Berven, MD**[c], **Wellington K. Hsu, MD**[d], **Thomas E. Mroz, MD**[e], and **Christian M. Puttlitz, PhD**[a]

[a]Department of Mechanical Engineering and School of Biomedical Engineering, Orthopaedic Bioengineering Research Laboratory, Colorado State University, 1374 Campus Delivery, 200 W Lake St, Fort Collins, CO 80523, USA

[b]Preclinical Surgical Research Laboratory (PSRL), Colorado State University, 300 W Drake Rd, Fort Collins, CO 80525, USA

[c]Department of Orthopedic Surgery, University of California San Francisco, San Francisco, CA 94142, USA

[d]Feinberg School of Medicine, Northwestern University, 420 E Superior St, Chicago, IL 60611, USA

[e]The Cleveland Clinic, 9500 Euclid Ave, Cleveland, OH 44195, USA

Abstract

BACKGROUND CONTEXT: There is significant variability in the materials commonly used for interbody cages in spine surgery. It is theorized that three-dimensional (3D)-printed interbody cages using porous titanium material can provide more consistent bone ingrowth and biological fixation.

PURPOSE: The purpose of this study was to provide an evidence-based approach to decisionmaking regarding interbody materials for spinal fusion.

STUDY DESIGN: A comparative animal study was performed.

METHODS: A skeletally mature ovine lumbar fusion model was used for this study. Interbody fusions were performed at L2-L3 and L4-L5 in 27 mature sheep using three different interbody cages (ie, polyetheretherketone [PEEK], plasma sprayed porous titanium-coated PEEK [PSP], and 3D-printed porous titanium alloy cage [PTA]). Non-destructive kinematic testing was performed in the three primary directions of motion. The specimens were then analyzed using micro-computed tomography (μ-CT); quantitative measures of the bony fusion were performed. Histomorphometric analyses were also performed in the sagittal plane through the interbody device. Outcome parameters were compared between cage designs and time points.

RESULTS: Flexion-extension range of motion (ROM) was statistically reduced for the PTA group compared with the PEEK cages at 16 weeks (p-value=.02). Only the PTA cages demonstrated a statistically significant decrease in ROM and increase in stiffness across all three loading directions between the 8-week and 16-week sacrifice time points (p-value .01). Micro-CT data demonstrated significantly greater total bone volume within the graft window for the PTA cages at both 8 weeks and 16 weeks compared with the PEEK cages (p-value<.01).

CONCLUSIONS: A direct comparison of interbody implants demonstrates significant and measurable differences in biomechanical, μ-CT, and histologic performance in an ovine model. The 3Dprinted porous titanium interbody cage resulted in statistically significant reductions in ROM, increases in the bone ingrowth profile, as well as average construct stiffness compared with PEEK and PSP.

Introduction

Circumferential fusion of the lumbar spine has been associated with improved clinical results and durability of the outcomes compared with posterolateral fusion in some series [1,2]. Interbody cages are useful in circumferential fusion to improve segmental stability, alignment of the spine, and interbody arthrodesis. Numerous interbody implants, made from metal, plastics, or composites, have been designed and used in clinical cases [3,4]; two of the most popular materials used for interbody spacers are titanium (Ti_6Al_4V) and polyetheretherketone (PEEK). Although interbody cages have been routinely used to achieve fusion for over a decade, existing designs fall short of providing all the necessary characteristics for clinical success. For example, although PEEK demonstrates durability and a Young modulus close to native bone, the material itself does not typically integrate into bone after implantation. Novel surface treatments for PEEK cages such as titanium plasma-spray and vapor deposition theoretically improve upon the properties of bone formation but have been found to have weak surface interface that can fracture upon cage implantation [5,6].

Existing metal cages may improve the opportunity for surface bone formation but may lead to subsidence and implant migration because of the mismatch in the biomechanical properties between the cage and the surrounding tissue. However, titanium interbody implants have been shown to be beneficial because they provide sufficient strength under physiological loads and have good biocompatibility [4,6,7]. Nevertheless, many surgeons are concerned with the clarity of the radiographic images when assessing the fusion mass and have also noted increased rates of subsidence of these implants due to a higher modulus of elasticity [8]. In contrast, PEEK implants are radiolucent, which allows for a clearer visualization of the interbody space and possibly improved assessment of interbody fusion on a variety of imaging modalities. However, PEEK has biochemical properties that are problematic regarding bone formation in the region of the implant. Also, PEEK is hydrophobic in nature and is unable to bond to bone to achieve a solid fusion, and may be associated with cage migration and pseudarthrosis [9].

Although both titanium and PEEK implants have been used widely as interbody cages, their function within the vertebral disc space is predominantly mechanical, and they require the addition of a biological or synthetic material to achieve bony fusion. With fusion-promoting innovations on the rise, one technique that has recently become popular is applying surface treatments or porous osteoconductive technologies to the superior and inferior surfaces of the cage to promote greater local osteoblast differentiation [5,10]. The application of these surface technologies to interbody fusion cages has the potential to increase the rate of fusion, while also creating an ultimately stronger fusion construct if the bony material is able to fully integrate into the cage. Additive manufacturing techniques, such as three-dimensional (3D) printing, can further enhance the biomechanical properties of a structural cage by titrating the porosity, strut widths, and orientation of surface modifications. These methods can improve upon conventional manufacturing protocols by reducing and enhancing relative stiffness in critical areas of a structural cage. Versatility in cage construction can optimize both the structure and biocompatibility of these devices simultaneously.

The recent development of a novel 3D-printed porous titanium cage was guided by the goals of improving osteointegration of the cage to the adjacent vertebra and improving the stability of the motion segment after healing. The purpose of this study was to compare the potential bony ingrowth and biomechanical differences following implantation of 3D-printed porous titanium cage with other interbody fusion cages with different surface technologies.

Materials and methods

Animal model justification

This study was performed under approval from the Institutional Animal Care and Use Committee at Colorado State University (protocol #: 15–5608A). A skeletally mature ovine lumbar fusion model was used for this study. The ovine model is an established one that has previously been used to evaluate spinal fusion in a preclinical setting [11–14].

Surgical approach and sample allocation

The L2 through L5 intervertebra! spaces were exposed using a left lateral retroperitoneal approach via a plane of dissection through the oblique abdominal muscles to the muscle plane ventral to the transverse processes. The L4-L5 and L2-L3 disk spaces were identified and annulotomies were performed. The medial portions of the annulus fibrosis and nucleus pulposus were removed with a pituitary rongeur. The intervertebral space was distracted to gain adequate exposure to the end plate surfaces. The end plates were prepared advancing a 6-mm drill across the disk space followed by further exposure with a high-speed burr to accommodate the appropriate interbody cage implant size. Once the intervertebral space was properly prepared, autologous iliac bone crest graft (approx. 0.33 cc of graft) was placed within the graft window of the cage and the cages were impacted into position. PEEK (7 × 11 × 20 mm; UniLIF PEEK; Stryker, Kalamazoo, MI, USA), plasma-sprayed porous titanium-coated PEEK (PSP) (7 × 10 × 22 mm; X-Spine Calix-PC; Stryker, Kalamazoo, MI, USA), and novel 3D-printed porous titanium alloy (PTA) (7 × 11 × 23 mm; Tritanium PL; Stryker, Kalamazoo, MI, USA) cages (height × length × width) with 0° of lordosis were used. Pedicle screws were placed into the central portion of the vertebral body in the dorsal plane and precut titanium rods were placed across the pedicle screws and secured with locking caps (XIA 3 Titanium Polyaxial Pedicle Screw System, Stryker Spine, Kalamazoo, MI, USA). Routine closure was performed. Following complete recovery, the sheep were allowed to eat and move ad libitum. The sheep were monitored daily throughout the study period for any signs of adverse events or complications, to evaluate pain, lameness, incisional site infection, neurologic status, and ambulatory function.

The location of each treatment variant was randomized with the condition that each animal was not implanted with two of the same cage types. Following euthanasia, lumbar spine segments were divided into individual functional spinal units (FSUs) and prepared for non-destructive biomechanical testing, micro-computed tomography (μ-CT) analysis, and histologic processing with histomorphometry. Twenty-seven (n=27) sheep were used for the study. Fifteen (eg, n=30 surgically treated FSUs; n=10 per group) animals were euthanized at 8 weeks and 12 (eg, n=24 surgically treated FSUs; n=8 per group) animals were euthanized at 16 weeks. It was theorized that by selecting two healing time points, it would be possible to detect differences in the biomechanical, radiographic, and histologic outcome parameters between treatments in the critically important acute healing phase.

Kinematic non-destructive range of motion testing

Non-destructive biomechanical tests were performed to determine the kinematic ranges of motion (ROMs) in the operated segments. The operated spinal motion segments were explanted immediately following sacrifice of the animals. Spines were cleaned of extraneous soft tissues, with care to preserve the bony and soft tissue architecture (ie, facet capsular ligaments, anterior longitudinal ligament, interspinous ligaments, and supraspinous ligament) around the fusion mass. The dorsal connecting rods were removed. Samples were kept hydrated via physiological saline spray at 10-minute intervals during the preparation and testing protocols. Following dissection, the distal ends of each FSU was potted in a strong two-part hard cast resin (SmoothCast 321, Smooth-On, Macungie, PA, USA) to insure proper mechanical fixation between the sample and the testing system. A custom-

built testing system was used to apply pure moments in the three principal kinematic directions (ie, flexion-extension, right-left lateral bending, and right-left axial rotation) without applying offset moments or shear forces. The testing fixture consisted of a servomotor actuator that applied moments in a specified direction and an aluminum frame to accommodate the potted specimen, load cell, and actuator. A six degree-of-freedom load transducer (AMTI, Watertown, MA, USA) was used to measure moments and shear forces throughout testing. A three-camera stereophotogrammetry system (Motion Analysis Corp, Santa Rosa, CA, USA) was used to track optical markers and determine the intervertebral ROM. Marker triads were placed at the tips of Kirschner wires, drilled into the vertebral bodies, and tracked by the three high-resolution cameras. Three-dimensional coordinates of the marker sets were recorded, and the related Euler angles for the relative motion at the implanted levels were calculated. All data were recorded at 100 Hz using a custom-written code (Labview 8.0, National Instruments Co, Austin, TX, USA).

The bending directions were randomly ordered for each specimen. Moments were applied to the cranial vertebral body using a sinusoidal waveform at a quasi-static rate (2.8°/s) until the specified torque was attained. All spines underwent five cycles of non-destructive loading with loads ranging from-6.0 Nm to 6.0 Nm in bending or torsion. The last data cycle was processed for the biomechanical analyses. Standard spine biomechanics parameters were measured or calculated for each loading mode. The parameters of interest were ROM, degrees (ROM, deg); construct stiffness (N-m/deg); and neutral zone (NZ, deg). Range of motion was calculated as the absolute difference between the maximum and minimum angles measured during the last loading cycle. Stiffness was calculated as the slope of the moment-ROM curve over the loading profile. Neutral zone was calculated as the magnitude between the loading and unloading curves at zero applied moment.

Micro-CT scanning and analyses

Following biomechanical testing, μ-CT scanning was completed on all specimens. Following at least 1 week of fixation in 10% neutral buffered formalin, specimens were trimmed superior to the superior pedicle screw hole and inferior to the inferior screw hole in the axial plane. The resultant tissue section encompassed the vertebral body end plates, the entire disc space, and the interbody device, as well as any resultant callus formation. The specimens were scanned at an isotropic resolution of 37 μ.m (Scanco μCT 80, Scanco USA Inc, Wayne, PA, USA). Quantitative measures of the graft window were performed, including bone volume/total volume (BV/ TV; expressed as a percentage (%)). The mean density of bone volume/mean density of total volume (MDBV/MDTV) was also calculated. As MDBV/MDTV approaches unity, then the region of interest (ROI) is considered to have a more solid architecture and is used to quantify the solidity of bone within the graft window. The ROI was set as a circular disc within the center of the cage, equally spaced from the cage's mediallateral, anterior-posterior, cranial-caudal boundaries. Morphometric indices were calculated using proprietary software (Scanco μCT 80, Scanco USA Inc).

Histology slide preparation and histomorphometry

All histology samples were processed for undecalcified histologic analyses. Following μ-CT, specimens were further trimmed to an approximately 1-cm thick section in the sagittal plane

located slightly off the centerline of the interbody device. These sections encompassed the superior and inferior end plate as well as the disc space and interbody device. After neutral buffered formalin fixation, the samples were dehydrated in graded solutions of ethyl alcohol on a tissue processor (Tissue-Tek VIP, Sakura, Torrance, CA, USA). After processing, the samples were cleared with acetone and polymerized into a hardened plastic block (Acrylosin, Dorn and Hart Microedge Inc, Villa Park, IL, USA). Histologic sections were taken in the sagittal plane through the interbody device to display the implant's core and anterior-posterior surfaces (ie, walls) and surrounding bone. Two slides were produced from each sample. Slides were first stained with Sanderson rapid bone stain, which provides differentiation of cells within the section and allows detection of cartilage within the tissue. Slides were then counterstained using a Van Gieson bone stain that allows differentiation of collagen and detection of bone (immature woven bone and mature lamellar bone) within the section.

Histomorphometric measurements were performed on calibrated digital images to quantify the percentage of new bone, implant, background space, and fibrous tissue within the histomorphometric ROI (Fig. 1) (ImagePro, Media Cybernetics, Silver Spring, MD, USA). The nomenclature "background" was used when the space did not contain the main constituents of interest (ie, bone, implant, and soft tissue) even though these areas still may have still contained bone marrow cells, blood cells, etc.

Stained histology sections were also evaluated by a certified pathologist to qualitatively document the cellular responses observed for each of the implanted cages. The pathologist was blinded to the treatment group. The sections were qualitatively analyzed according to cell type (ie, polymorphonuclear, lymphocytes, plasma, macrophages, giant, and osteoblastic cells) and responses (ie, signs of bone remodeling, implant degradation, and neovascularization).

Statistical analyses

Following data processing, statistical analyses were performed on all outcome parameters. Standard two-way analyses of variance were performed to determine statistically significant differences (p .05) within and across treatment groups (SigmaSTAT, Systat Software Inc, San Jose, CA, USA). The treatment type and sacrifice time point represented the two levels within each statistical analysis. A Student-Newman-Keuls (SNK) post hoc test was implemented when statistically significant differences were detected.

Results

No grossly abnormal pathologies or abnormal tissue reactions were noted at the time of dissection. No experimental issues were noted; all biomechanical tests were run to completion.

Data figures are shown in box and whisker plot format. The "box" is bounded by the first and third quartiles; the "whiskers" represent the maximum or minimum values within the data set, and the median data bar is highlighted. Statistically significant differences have

been highlighted; similar roman letters indicate differences between treatment groups with the specific p-values given.

Kinematic non-destructive testing results

No significant differences within the 8-week or the 16-week sacrifice time points were noted between the treatment groups for axial rotation ROM (Fig. 2A; p=.44 and .92, respectively), stiffness (p=.31 and .71, respectively; Fig. 2D), or NZ (p=.93 and .37, respectively; Table). The PTA group demonstrated statistically significant greater axial ROM at 8 weeks compared with the PEEK, PSP, and PTA groups at the 16-week time sacrifice point (p=.03, .03, and .02, respectively; Fig. 2A). A significant temporal increase in stiffness was observed under axial rotation for the PEEK, PSP, and PTA groups compared with the 8-week PTA group (p=.05, <.01, and <.01, respectively; Fig. 2D). Reductions in NZ were noted for the 16-week PEEK samples compared with the 8-week PEEK, PSP, and PTA groups (p<.01, .03 and .01, respectively; Table). The 16-week PTA treatment also demonstrated significant reductions in NZ compared with the 8-week PEEK, PSP, and PTA groups (p<.05, .03, and .01, respectively; Table). The 16-week PSP group demonstrated significant NZ reduction compared with the 8-week PEEK group only (p=.05; Table).

No significant differences within the 8-week time point was noted between the treatment groups for flexion-extension ROM (Fig. 2B; p=.12). However, a significant decrease in ROM under flexion-extension ROM was observed for the PTA group compared with the PEEK group within the 16-week sacrifice time point (p=.04; Fig. 2B). The 16-week PTA treatment also demonstrated significantly less flexion-extension ROM compared with the 8-week PEEK, PSP, and PTA treatments (p=.04, .01, and <.01, respectively; Fig. 2B). The 16-week PSP group showed significant temporal reductions in flexion-extension ROM from the 8-week to the 16-week time point (p=.05; Fig. 2B). No significant differences were noted between the two treatment groups for flexion-extension stiffness within the 8-week or 16-week sacrifice time points (p=.20 and .09, respectively; Fig. 2E). However, the PTA group did demonstrate statistically significant increase in flexion-extension stiffness compared with the PSP and PEEK treatments at 8 weeks (p<.01 for both comparisons; Fig. 2E). Reductions in NZ were observed within the 8-week sacrifice time point for the PTA treatment compared with the PSP group (p=.04; Table). No significant differences in NZ were noted between the treatment groups within the 16-week sacrifice time points under flexion-extension (p=.11; Table). The 8-week PSP group had statistically greater NZ compared with the 16-week PEEK, PTA, and PSP treatments (p<.04, <.01, and .01, respectively; Table). The 8-week PEEK group demonstrated greater NZ compared with the 16-week PTA treatment (p=.03; Table).

No significant differences were noted between the treatment groups for lateral bending ROM within the 8-week or 16-week sacrifice time points (p=.88 and .71, respectively; Fig. 2C). The PTA group demonstrated statistically significant lower lateral bending ROM at 16 weeks compared with the PEEK, PSP, and PTA groups at the 8-week time sacrifice point (p=.01, <.01, and <.01, respectively; Fig. 2C). The PEEK treatment at 16 weeks demonstrated a significant reduction in lateral bending ROM compared with the PSP and PTA treatments at 8 weeks (p=.02 and .03, respectively; Fig. 2C). The 16-week PSP group

demonstrated significant lateral bending ROM reduction compared with the 8-week PSP group only (p=.05; Fig. 2C). A significant temporal increase in stiffness was observed for the PTA group under lateral bending (p=.02; Fig. 2F). The 8-week PSP treatment demonstrated significantly less lateral bending stiffness compared with the PEEK, PSP, and PTA 16-week samples (p=.02, .03, and <.01, respectively; Fig. 2F). No differences in NZ were noted across the treatment groups under lateral bending within the 8-week or 16-week sacrifice time points (p=.15 and .64 respectively; Table). The PSP treatment at 8 weeks exhibited a significantly greater lateral bending NZ compared with the 16-week PEEK and PTA groups (p=.02 and <.01, respectively; Table).

Micro-CTanalyses results

Sample μ-CT 3D renderings in the coronal (Fig. 3A) and midsagittal (Fig. 3B) planes of the interbody device at the 8-week and 16-week sacrifice time points are shown. Significant increases were observed in BV/TV for the PTA group compared with the PEEK and PSP groups at both the 8-week and 16-week sacrifice time points (p<.01 for all comparisons; Fig. 3C). The PTA treatment at 16 weeks also demonstrated significantly greater BV/TV compared with the PEEK and PSP treatments at 8 weeks (p=.01 and <.01, respectively; Fig. 3C). The 16-week PTA treatment demonstrated significantly lowered BV/TV compared with the 8-week PTA samples (p=.02; Fig. 3C).

A significantly greater MDBV/MDTV ratio was observed for the PTA group compared with the PEEK and PSP groups within the 8-week sacrifice time point (p<.01 and .02, respectively; Fig. 3D). The PTA treatment also indicated a higher MDBV/MDTV ratio compared with the PSP samples within the 16-week sacrifice time point (p<.01; Fig. 3D). No significant differences in the MDBV/MDTV ratio were observed across sacrifice time points for any comparisons (p=.06; Fig. 3D)

Histomorphometry results

No significant differences in the total area (mm^2) of the ROI were calculated within or across treatments and sacrifice time points (p=.73; data not shown).

The differences in the percent bone within the histomorphometry ROI indicated a significant increase in the PTA group at 16 weeks compared with the PEEK, PSP, and PTA treatments at the 8-week sacrifice time point (p<.01 for all comparisons; Fig. 4A). The PTA treatment at 16 weeks also demonstrated a significantly increased percent bone compared with the 16-week PEEK group (p=.04; Fig. 4A).

The PTA group at both the 8-week and 16-week time points had significantly less percent implant within the ROI compared with the PEEK and PSP treatments at both the 8-week and 16-week time points (p<.01 for all comparisons; Fig. 4B).

No significant difference in the percent soft tissue were calculated across sacrifice time points or within treatment variants (p=.41; Fig. 4C). Similarly, no significant difference in the percent background were calculated across sacrifice time points or within treatment variants (p=.41; Fig. 4D).

For completeness, the percent (means±standard deviations) bone ingrowth into the available space within the porous architecture of the PTA implant was calculated to be 20.11%±6.31% and 24.10%±8.40% at 8 weeks and 16 weeks, respectively. The percent soft tissue into the porous architecture of the PTA was also calculated to be 46.71%±8.31% and 35.09%±7.31% at 8 weeks and 16 weeks, respectively. The percent background into the porous architecture of the PTA was calculated to be 21.30%±5.50% and 14.42%±4.35% at 8 weeks and 16 weeks, respectively. Bone, soft-tissue, and background ingrowth were not measured for the PEEK or PSP samples as these devices were solid (Fig. 1).

Histopathology results

In almost all cases, the inter-implant defect, regardless of the implant type, was predominately filled with new reactive or woven bone, admixed with far lesser amounts of cartilage and dense fibrous connective tissue. This new bone frequently bridged the graft window space. Cases in which there was not complete bony bridging were typically due to the presence of lobules of cartilage which were still undergoing the process of remodeling and ossification.

All three implant types were frequently intimately encapsulated by a reactive fibrous capsule of varying thickness and density. There appeared to be a slight association of the PTA implants with having less encapsulation or fibrosis and having increased amounts of reactive bone directly in contact with the implant surface replacing the fibrous capsule. However, these findings were variable and all three types of implants displayed a large variability in the amount of bone versus fibrous connective tissue in contact with their surface.

Overall, the PEEK implants appeared to be associated with an increased amount of poorly vascularized fibrous connective tissue surrounding the implant, as well as a mildly increased inflammatory response, typically composed of lymphocytes and macrophages, compared with the PTA and PSP groups. All the PEEK samples demonstrated a moderate to significant degree of the "PEEK-halo" effect.

The PSP implants appeared to be associated with a slightly decreased amount of fibrous connective tissue surrounding the implant, as well as a mildly decreased inflammatory response compared with animals in the PEEK group. In addition, the fibrous connective tissue surrounding the implants in the PSP group appeared to have a slight increase in neovascularization. Osteoblast activity and osteoclastic remodeling appeared slightly increased in this PTA group compared with both the PEEK and PSP groups. Therefore, given the lack of fibrous connective tissue surrounding the PTA implant (and thus greater degree of surface contact between new reactive bone and the implant), in conjunction with bony filling of the implant pores and complete bony bridging of the defect at multiple levels, the integration of these implants into the vertebral bodies and the overall bridging of the defect appeared qualitatively more uniform in continuity in this group compared with the PEEK and PTA groups. The pores of the PTA implants were filled with either fibrous connective tissue or reactive new bone, and lesser amounts of cartilage. Proportion of the filling by these tissue types was variable between individuals and varied within portions of the implant. Areas of porous implant that were filled with new bone also demonstrated surfaces of the porous implants that were completely encapsulated in new bone.

Conclusions

The data presented in this study provide an evidence-based approach to aid in the decision-making regarding interbody materials for spinal fusion. These data were important because interbody implant surface materials have a significant and measurable impact on the biomechanics of the fused motion segment and on the osseointegration of the interbody device and vertebral end plates [15–17]. PEEK has been widely used as an implant material for spinal fusion because of its good mechanical properties, low density (ie, radiolucency), and good chemical resistance [18]. However, PEEK alone is chemically inert, forming a biofilm layer that inhibits binding to the host bone, which has limited its wider application [19]. Therefore, to achieve interbody fusion with PEEK, bone must grow around the cage. Many attempts have been made to overcome the limitations of PEEK; coating PEEK with a bioactive substance has been shown to be a very effective technique for enhancing the biocompatibility of PEEK, while maintaining its other advantages [20–23]. Titanium is one of the most common metals used to augment PEEK's performance in spinal fusion [24]. However, recent studies have demonstrated that implantation of titanium-coated PEEK are susceptible to impaction-related wear debris [25]. Titanium wear debris causes biological reactions in the human body, and local inflammatory reactions have been reported in various animal and clinical studies [26–28]. However, it remains unclear whether the amount of wear after impaction and the resulting tissue concentration of these particles are high enough to cause postoperative complications [25].

It is theorized that the risk of delamination and wear debris is significantly reduced in solid or 3D-printed metal cages because of the lack of an interface between two materials of different moduli (ie, PEEK and titanium). It has also been previously shown that porous titanium implants create an osteoconductive surface that provides short-term stability due to friction and long-term stability due to cell adhesion leading to bony ongrowth (ie, direct apposition of bone onto the surface of the implant) and ingrowth (ie, bone formation within the irregular porous architecture of the implant) [19]. Further, it has also been demonstrated that cells more widely proliferate and differentiate on titanium than PEEK [17]. This is most likely because of titanium's osseointegration properties; in fact, many past studies have shown that titanium implants demonstrate good bone-to-implant contact and osteogenic properties during fusion processes [5,29,30]. Yet, a need still exists to examine how these interbody fusion materials can be most effectively used for spinal fusion, given the mixed results of previous studies with minimal evidence for better clinical and radiographic outcomes were found for a variety of cage materials [31,32].

The results of the present study demonstrate the potential for bone ingrowth into the PTA cage itself, as well as bone growth around the cage. The ingrowth seen with porous titanium alloy was superior to that seen with both PEEK and plasma spray-coated implants. A potential benefit of ingrowth includes improved construct stability, as demonstrated by the biomechanical findings in this study. The main benefits of PTA noted in this study were the ability of bone to grow within the 3D architecture of the device, ultimately resulting in superior kinematic properties (ie, reduction in ROM and increases in stiffness). Our histomorphometric data demonstrated osteoblastic deposition within the porous network of the PTA devices and significantly increased overall percentage of bone within the ROI at 16

weeks compared with the other devices. The histomorphometric observations of 20%–24% bone ingrowth into the available space of the porous titanium cage indicate that peri-implant osteogenesis is occurring. Peri-implant osteogenesis is known to be a multistep process that includes osteoblast adhesion to the surface of a material, proliferation and differentiation (involving the production of specific proteins), and deposition of calcium phosphate in the extracellular matrix [33]. These data mirror the findings of previously reported computational and comparative animal studies that have also demonstrated that bone ingrowth into porous titanium cages results in increased implant stability [7,34,35]. The data suggest that by providing a microporous construct of titanium, bony ongrowth or ingrowth may occur, leading to greater overall mechanical construct stability and efficacy as a fusion-promoting device.

Our data mirror the findings of previously reported computational and comparative animal studies that have also demonstrated that bone ingrowth into porous titanium implants results in increased implant stability [7,34,35]. The data suggest that in a microporous titanium implant, cells may form bony ongrowth on the surface and ingrowth into the middle of the implant, leading to greater overall mechanical construct stability and efficacy as a fusion-promoting device. These data indicate that there are distinct clinical advantages (eg, reductions in ROM, increases in fusion site stiffness) to incorporating the biological properties of microporous titanium (osteoconduction, cell binding) into spinal fusion devices.

Owing to the similarities (ie, anatomical features, in vivo biomechanical loading, bone composition or structure, etc.) between humans and sheep [36–41], we believe that it is acceptable to conjecture that increased fusion results between treatment groups detected within this study in the in vivo ovine model would correspond to the increases in fusion results observed between treatment groups in human subjects. However, we realize that a limitation of this study is that these results have not been assessed for human clinical benefit in a large human patient population. Future, retrospective studies in large patient populations would ultimately be needed to determine the response of the devices' effects on outcome or quality of life postoperatively in human subjects.

Nevertheless, this study clearly demonstrates that the porous titanium microstructure of the PTA implant reliably bonds to the vertebral end plates by bony ingrowth and ongrowth. These data support the added benefit of PTA cages to promote biological bonding of the actual cage to the host bone, in addition to bone growth throughout the central portion of the implant. Thus, successful fusion is not relying only on the relative strength of bone growth through the graft window, but additionally upon the biological bonding of the implant to the host bone. These data support the kinematic and histologic benefits of PTA cages to promote biological bonding of the cage to the host bone in addition to bone growth through the central portion of the implant.

The clinical value of improved osteointegration of the interbody cage and improved segmental stiffness has yet to be demonstrated in prospective clinical study. One purpose of an interbody fusion cage is to contribute directly to the stiffness of the motion segment and to a solid bony union between adjacent vertebrae. This study provides a direct comparison of

commonly used materials for interbody fusion and offers useful information to guide informed choice regarding interbody devices.

Acknowledgment

References

[1]. Han X, Zhu Y, Cui C, et al. A meta-analysis of circumferential fusion versus instrumented posterolateral fusion in the lumbar spine. Spine 2009;34:E618–25. [PubMed: 19644321]

[2]. Soegaard R, Bunger CE, Christiansen T, et al. Circumferential fusion is dominant over posterolateral fusion in a long-term perspective: cost-utility evaluation of a randomized controlled trial in severe, chronic low back pain. Spine 2007;32:2405–14. [PubMed: 18090078]

[3]. Bagby GW. Arthrodesis by the distraction-compression method using a stainless-steel implant. Orthopedics 1988;11:931–4. [PubMed: 3387340]

[4]. Rao PJ, Pelletier MH, Walsh WR, et al. Spine interbody implants: material selection and modification, functionalization and bioactivation of surfaces to improve osseointegration. Orthop Surg 2014;6:81–9. [PubMed: 24890288]

[5]. Olivares-Navarrete R, Gittens RA, Schneider JM, et al. Osteoblasts exhibit a more differentiated phenotype and increased bone morphogenetic protein production on titanium alloy substrates than on poly-ether-ether-ketone. Spine J 2012;12:265–72. [PubMed: 22424980]

[6]. Olivares-Navarrete R, Hyzy SL, Slosar PJ, et al. Implant materials generate different peri-implant inflammatory factors: poly-ether-ether-ketone promotes fibrosis and microtextured titanium promotes osteogenic factors. Spine 2015;40:399–404. [PubMed: 25584952]

[7]. Guyer RD, Abitbol JJ, Ohnmeiss DD, et al. Evaluating osseointegration into a deeply porous titanium scaffold: a biomechanical comparison with PEEK and allograft. Spine 2016;41:E1146–50. [PubMed: 27135643]

[8]. Niu CC, Liao JC, Chen WJ, et al. Outcomes of interbody fusion cages used in 1 and 2-levels anterior cervical discectomy and fusion: titanium cages versus polyetheretherketone (PEEK) cages. J Spinal Disord Tech 2010;23:310–16. [PubMed: 20124907]

[9]. Duncan JW, Bailey RA. An analysis of fusion cage migration in unilateral and bilateral fixation with transforaminal lumbar interbody fusion. Eur Spine J 2013;22:439–45. [PubMed: 22878377]

[10]. Olivares-Navarrete R, Hyzy SL, Gittens RA, 1st, et al. Rough titanium alloys regulate osteoblast production of angiogenic factors. Spine J 2013;13:1563–70. [PubMed: 23684238]

[11]. Gadomski BC, McGilvray KC, Easley JT, et al. An in vivo ovine model of bone tissue alterations in simulated microgravity conditions. J Biomech Eng 2014;136:021020. [PubMed: 24170133]

[12]. Gadomski BC, McGilvray KC, Easley JT, et al. Partial gravity unloading inhibits bone healing responses in a large animal model. J Biomech 2014;47:2836–42. [PubMed: 25138631]

[13]. Lindley EM, Barton C, Blount T, et al. An analysis of spine fusion outcomes in sheep pre-clinical models. Eur Spine J 2016.

[14]. McGilvray KC, Waldorff EI, Easley J, et al. Evaluation of a PEEK titanium composite interbody spacer in an ovine lumbar interbody fusion model: a biomechanical, micro-computed tomography, and histologic analyses. Spine J 2017.

[15]. Pelletier MH, Cordaro N, Punjabi VM, et al. PEEK versus Ti interbody fusion devices: resultant fusion, bone apposition, initial and 26-week biomechanics. Clin Spine Surg 2016;29:E208–14. [PubMed: 22801456]

[16]. Phan K, Hogan JA, Assem Y, et al. PEEK-Halo effect in interbody fusion. J Clin Neurosci 2016;24:138–40. [PubMed: 26474500]

[17]. Wu SH, Li Y, Zhang YQ, et al. Porous titanium-6 aluminum-4 vanadium cage has better osseointegration and less micromotion than a poly-ether-ether-ketone cage in sheep vertebral fusion. Artif Organs 2013;37:E191–201. [PubMed: 24147953]

[18]. Han CM, Lee EJ, Kim HE, et al. The electron beam deposition of titanium on polyetheretherketone (PEEK) and the resulting enhanced biological properties. Biomaterials 2010;31:3465–70. [PubMed: 20153890]

[19]. Yoon BJ, Xavier F, Walker BR, et al. Optimizing surface characteristics for cell adhesion and proliferation on titanium plasma spray coatings on polyetheretherketone. Spine J 2016;16:1238–43. [PubMed: 27241209]

[20]. Wu GM, Hsiao WD, Kung SF. Investigation of hydroxyapatite coated polyether ether ketone composites by gas plasma sprays. Surf Coat Technol 2009;203:2755–8.

[21]. Yu S, Hariram KP, Kumar R, et al. In vitro apatite formation and its growth kinetics on hydroxyapatite/polyetheretherketone biocomposites. Biomaterials 2005;26:2343–52. [PubMed: 15585237]

[22]. Yao C, Storey D, Webster TJ. Nanostructured metal coatings on polymers increase osteoblast attachment. Int J Nanomedicine 2007;2:487–92. [PubMed: 18019846]

[23]. Ha SW, Kirch M, Birchler F, et al. Surface activation of polyetheretherketone (PEEK) and formation of calcium phosphate coatings by precipitation. J Mater Sci Mater Med 1997;8:683–90. [PubMed: 15348819]

[24]. Jain S, Eltorai AE, Ruttiman R, et al. Advances in spinal interbody cages. Orthop Surg 2016;8:278–84. [PubMed: 27627709]

[25]. Kienle A, Graf N, Wilke HJ. Does impaction of titanium-coated interbody fusion cages into the disc space cause wear debris or delamination? Spine J 2016;16:235–42. [PubMed: 26409208]

[26]. Cunningham BW, Orbegoso CM, Dmitriev AE, et al. The effect of spinal instrumentation particulate wear debris: an in vivo rabbit model and applied clinical study of retrieved instrumentation cases. Spine J 2003;3:19–32. [PubMed: 14589241]

[27]. Cunningham BW, Orbegoso CM, Dmitriev AE, et al. The effect of titanium particulate on development and maintenance of a posterolateral spinal arthrodesis: an in vivo rabbit model. Spine 2002;27:1971–81. [PubMed: 12634556]

[28]. Kim H-D, Kim K-S, Ki S-C, et al. Electron microprobe analysis and tissue reaction around titanium alloy spinal implants. Asian Spine J 2007;1:1–7. [PubMed: 20411145]

[29]. Stenport VF, Johansson CB. Evaluations of bone tissue integration to pure and alloyed titanium implants. Clin Implant Dent Relat Res 2008;10:191–9. [PubMed: 18241219]

[30]. De Leonardis D, Garg AK, Pecora GE. Osseointegration of rough acid-etched titanium implants: 5-year follow-up of 100 minimatic implants. Int J Oral Maxillofac Implants 1999;14:384–91. [PubMed: 10379112]

[31]. Kersten RF, van Gaalen SM, de Gast A, et al. Polyetheretherketone (PEEK) cages in cervical applications: a systematic review. Spine J 2015;15:1446–60. [PubMed: 24374100]

[32]. Seaman S, Kerezoudis P, Bydon M, et al. Titanium vs. polyetheretherketone (PEEK) interbody fusion: meta-analysis and review of the literature. J Clin Neurosci 2017;44:23–9. [PubMed: 28736113]

[33]. Sagomonyants KB, Jarman-Smith ML, Devine JN, et al. The in vitro response of human osteoblasts to polyetheretherketone (PEEK) substrates compared to commercially pure titanium. Biomaterials 2008;29:1563–72. [PubMed: 18199478]

[34]. Lee YH, Chung CJ, Wang CW, et al. Computational comparison of three posterior lumbar interbody fusion techniques by using porous titanium interbody cages with 50% porosity. Comput Biol Med 2016;71:35–45. [PubMed: 26874064]

[35]. Tsou H-K, Chi M-H, Hung Y-W, et al. In vivo osseointegration performance of titanium dioxide coating modified polyetheretherketone using arc ion plating for spinal implant application. Biomed Res Int 2015.

[36]. Schmidt-Nielsen K Animal physiology: adaptation and environment. NewYork: Cambridge University Press; 1977.

[37]. Kettler A, Liakos L, Haegele B, et al. Are the spines of calf, pig and sheep suitable models for pre-clinical implant tests? Eur Spine J 2007;16:2186–92. [PubMed: 17721711]

[38]. Pearce AI, Richards RG, Milz S, et al. Animal models for implant biomaterial research in bone: a review. Eur Cell Mater 2007;13:1–10. [PubMed: 17334975]

[39]. Sheng SRX, Wang Y, Xu HZ, et al. Anatomy of large animal spines and its comparison to the human spine: a systematic review. Eur Spine J 2010;19:46–56. [PubMed: 19876658]

[40]. Wilke HJ, Kettler A, Claes LE. Are sheep spines a valid biomechanical model for human spines? Spine 1997;22:2365–74. [PubMed: 9355217]

[41]. Wilke HJ, Kettler A, Wenger KH, et al. Anatomy of the sheep spine and its comparison to the human spine. Anat Rec 1997;247:542–55. [PubMed: 9096794]
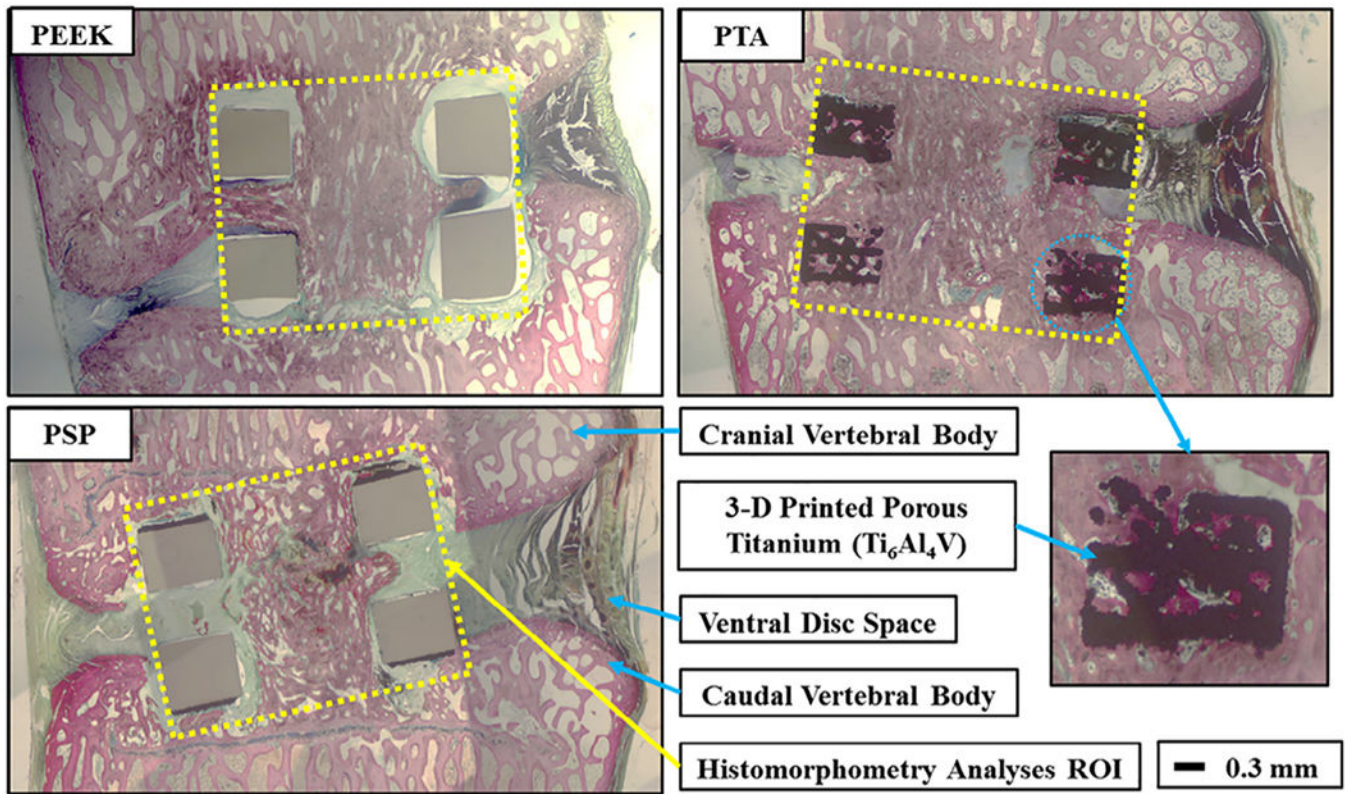
Fig. 1.
Digital image showing typical histologic sections taken in the sagittal plane through the cranial and caudal vertebral bodies including the surgically treated disc space for each treatment variant. These sample images are from the 16-week sacrifice time point. The ROI analysis (outlined with yellow dots) encompasses the entire implant. Measured parameters included the amount (%) of bone, fibrous tissue, implant, and "background" within each ROI. These images are coded as follows: bone stained, red; fibrous tissue, gray; implant, black (metal) or tan (plastic); and background, white. PEEK, polyetheretherketone; PSP, plasma sprayed porous titanium-coated PEEK; PTA, porous titanium alloy; ROI, region of interest.
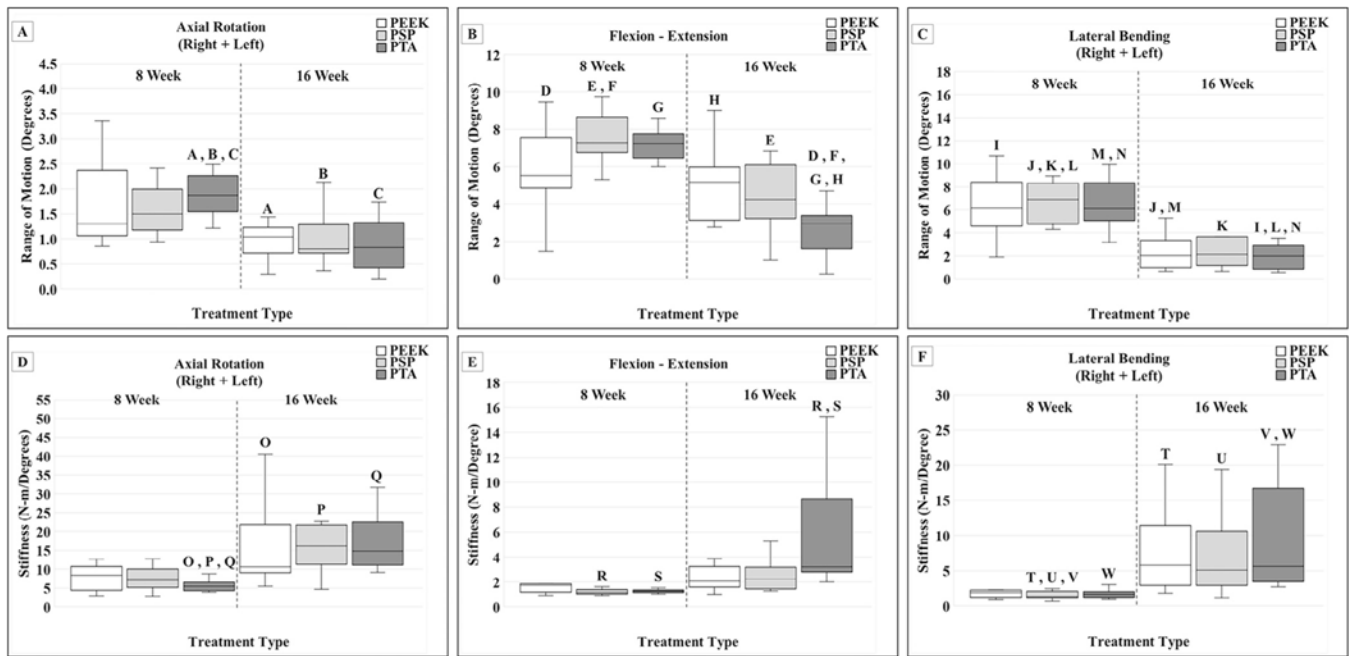
Fig. 2.

Range of motion (Top) and stiffness (Bottom) data collected during non-destructive pure moment loading. (A) Significant decreases in ROM under axial rotation were observed for the PEEK, PSP, and PTA groups at the 16-week time point compared with the PTA 8-week group (**A**, **C**: p=.03; **B**: p=.02). (B) Significant decreases in ROM under flexion-extension were observed for the PTA group at 16 weeks compared with all treatments at the 8-week sacrifice time point (**D**: p=.04; **F**: p=.01; **G**: p<.01). The PSP group demonstrated significant temporal decreases from 8 weeks to 16 weeks in flexion-extension ROM (**E**: p=.05). With the 16-week time point, the PTA group also had significantly less flexion-extension ROM compared with the PEEK treatment (**H**: p=.04). (C) Significant decreases in ROM under lateral bending were observed for the PTA group at 16 weeks compared with all treatments at the 8-week sacrifice time point (**I**: p=.01; **N**, **L**: p<.01). The PEEK group demonstrated significant temporal decreases from 8 weeks to 16 weeks in lateral bending ROM compared with the PEEK and PTA treatments (**J**: p=.02; **M**: p=.03). The PSP group demonstrated significant temporal decreases from 8 weeks to 16 weeks in lateral bending ROM (**K**: p=. 05). (D) Significant increases in stiffness were observed under axial rotation for all 16-week groups compared with the 8-week PTA treatment (**O**: p=.05; **P**, **Q**: p<.01). (E) Significant increases in stiffness under flexion-extension were observed for the PTA group at the 16-week time point compared with the PSP and PTA 8-week groups (**R**, **S**: p<.01). (F) Significant increases in stiffness under lateral bending were observed for all 16- week groups compared with the 8-week PSP treatment (**T**: p=.02; **U**; p=.03; **V**: p<.01). The PTA group demonstrated significant temporal increase from 8 weeks to 16 weeks in lateral bending stiffness (**W**: p=.02). PEEK, polyetheretherketone; PSP, plasma sprayed porous titanium-coated PEEK; PTA, porous titanium alloy; ROM, range of motion.
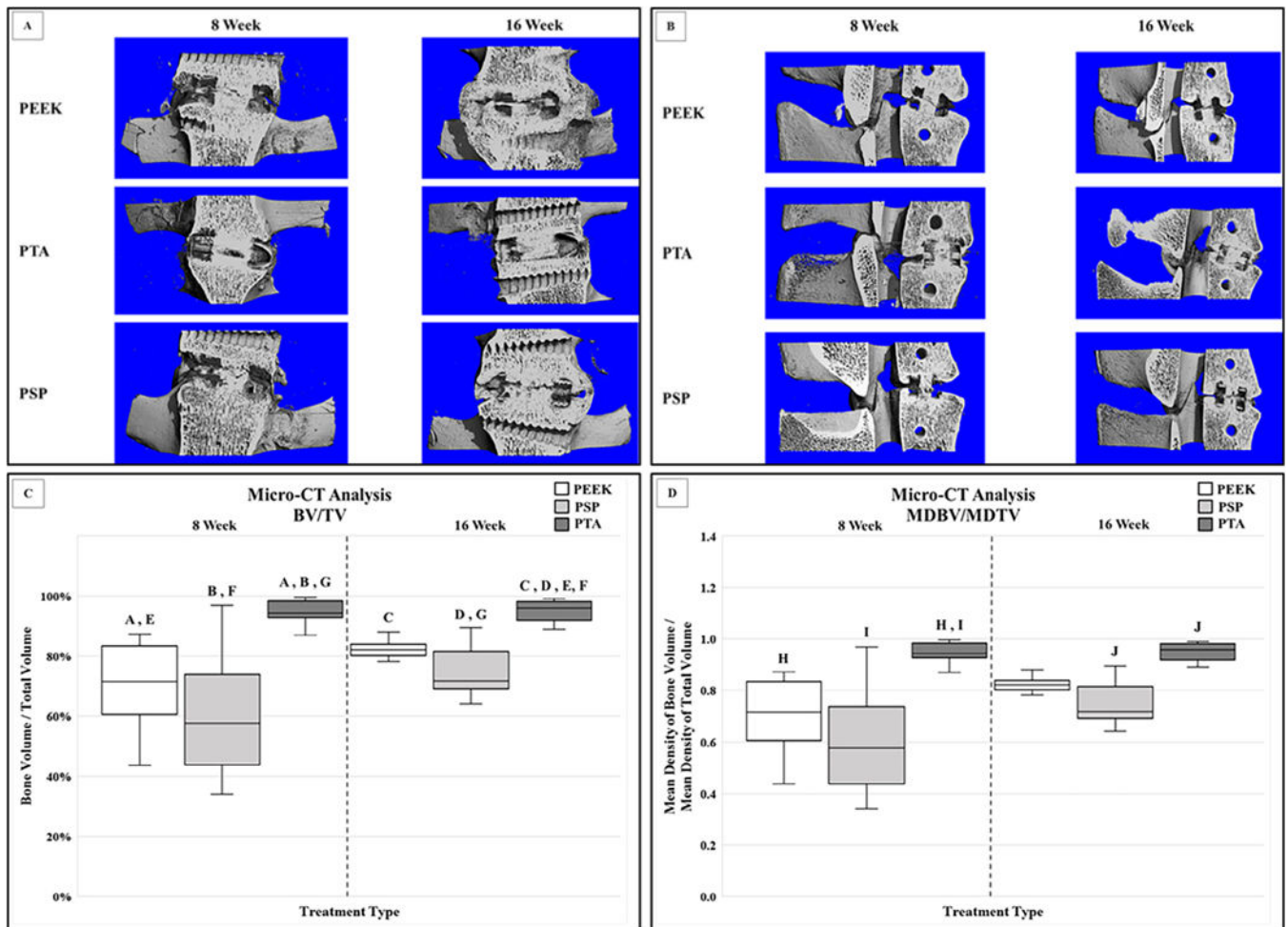
Fig. 3.
Example of μ-CT 3D renderings in the coronal (A) and midsagittal (B) planes of the interbody device at the 8-week and 16-week sacrifice time points. (C) Significant increases were observed in BV/TV for the PTA group compared with the PEEK and PSP groups at both the 8-week and 16-week sacrifice time points (**A**, **B**, **C**, **D**: p<.01). The PTA treatment at 16 weeks also demonstrated significantly greater BV/TV compared with the PEEK and PSP treatments at 8 weeks (**E**: p=.01; **F** p<.01). The 16-week PTA treatment demonstrated significantly lowered BV/TV compared with the 8-week PTA samples (**G**: p=.02). (D) A significantly greater MDBV/MDTV ratio was observed for the PTA group compared with the PEEK and PSP groups at the 8-week sacrifice time points (**H**: p<.01; **I**: p=.02). The PTA treatment also indicated a higher MDBV/MDTV ratio compared with the PSP samples within the 16-week time point (**J**: p<.01). BV/TV, bone volume/total volume; CT, computed tomography; MDBV/MDTV, mean density of bone volume/mean density of total volume; PEEK, polyetheretherketone; PSP, plasma sprayed porous titanium-coated PEEK; PTA, porous titanium alloy; ROM, range of motion.
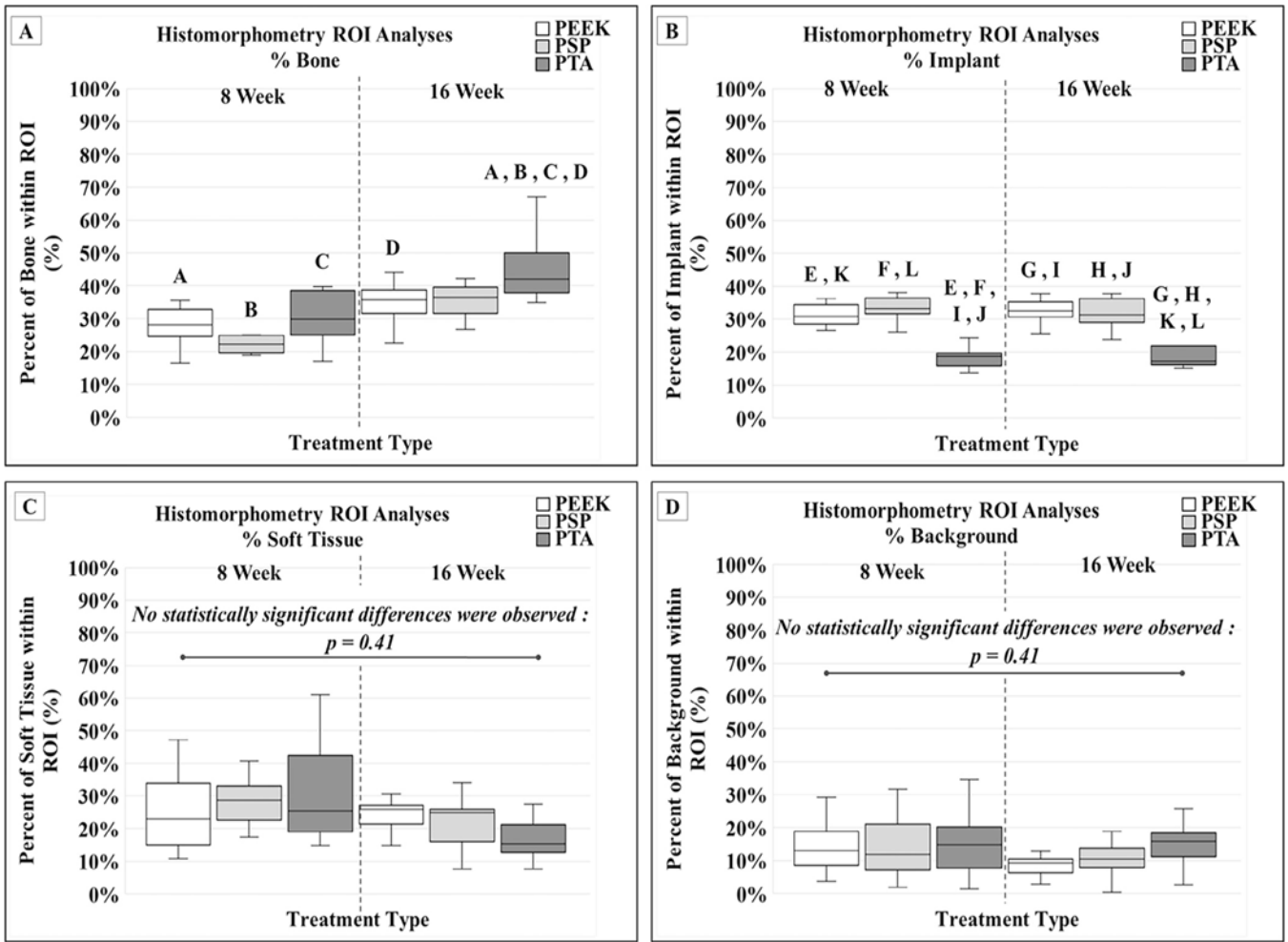
Fig. 4.
Histomorphometric parameters collected from midsagittal sections of the FSU. (A) A significant increase in the PTA group at 16 weeks compared with the PEEK, PSP, and PTA treatments at the 8-week sacrifice time point (**A, B, C**: p<.01). The PTA treatment at 16 weeks also demonstrated a significantly increased percent bone compared with the 16-week PEEK group (**D**: p=.04). (B) The PTA group at both the 8-week and 16-week time points had significantly less percent implant within the ROI compared with the PEEK and PSP treatments at both the 8-week and 16-week time points (**E, F, G, H, I, J, K, L**: p<.01). (C) No significant difference in the percent soft tissue were calculated across sacrifice time points or within treatment variants (p=.41). (D) No significant difference in the percent background were calculated across sacrifice time points or within treatment variants (p=.41). FSU, functional spinal unit; PEEK, polyetheretherketone; PSP, plasma sprayed porous titanium-coated PEEK; PTA, porous titanium alloy; ROI, region of interest.

Table

Neutral zone (degrees) calculated during non-destructive pure moment loading

Neutral zone (degrees)				
Treatment	**Time point**	**Axial rotation**	**Flexion-extension**	**Lateral bending**
PEEK	8 wk	$0.15 \pm 0.05^{A,D\,G}$,	0.67 ± 0.14^{J}	0.62 ± 0.14
PSP	8 wk	$0.19 \pm 0.06^{B,E}$	$1.08 \pm 0.14^{H,I,K,L}$	$0.79 \pm 0.10^{M,N}$
PTA	8 wk	$0.17 \pm 0.05^{C,F}$	0.58 ± 0.14^{H}	0.41 ± 0.15
PEEK	16 wk	$0.00 \pm 0.00^{A,B,C}$	0.37 ± 0.12^{I}	0.19 ± 0.11^{M}
PSP	16 wk	0.04 ± 0.04^{G}	0.40 ± 0.19^{I}	0.28 ± 0.13
PTA	16 wk	$0.00 \pm 0.00^{D,E,F}$	$0.05 \pm 0.05^{J,K}$	0.14 ± 0.07^{N}

PEEK, polyetheretherketone; PSP, plasma sprayed porous titanium-coated PEEK; PTA, porous titanium alloy.

Data means are shown with standard deviations; values with similar roman letters indicate statistically significant differences. Significant p-values are given below:

Axial rotation—

A: $p < .01$;

B: $p = .03$;

C: $p = .01$;

D: $p < .01$;

E: $p = .03$;

F: $p = .01$;

G: $p = .05$.

Flexion-extension—

H: $p = .04$;

I: $p < .01$;

J: $p = .03$;

K: $p < .01$;

L: $p = .01$.

Lateral bending—

M: $p = .02$;

N: $p < .01$.